Segmentation of Salt Solution and Hydrated Salt Crystals in Porous Limestone

Hannelore Derluyn[1,2], Matthieu N. Boone[3,4], Jan Dewanckele[4,5], Veerle Cnudde[4,5], Dominique Derome[2] and Jan Carmeliet[1,2]

[1]ETH Zurich, Chair of Building Physics, Wolfgang-Pauli-Strasse 15, 8093 Zürich Hönggerberg, Switzerland [email: derluyn@arch.ethz.ch; carmeliet@arch.ethz.ch]

[2]EMPA, Swiss Federal Laboratories for Materials Science and Technology, Laboratory for Building Science and Technology, Überlandstrasse 129, 8600 Dübendorf, Switzerland [email: hannelore.derluyn@empa.ch; dominique.derome@empa.ch; jan.carmeliet@empa.ch]

[3]Ghent University, Department of Physics and Astronomy, Faculty of Sciences, Proeftuinstraat 86, 9000 Gent, Belgium [email: Matthieu.Boone@UGent.be]

[4]Centre for X-ray Tomography, Institute for Nuclear Sciences, UGCT, Proeftuinstraat 86 9000 Gent, Belgium [email: UGCT@UGent.be]

[5]Ghent University, Department of Geology and Soil Science, Faculty of Sciences, Krijgslaan 281, S8, 9000 Gent, Belgium [email: Jan.Dewanckele@UGent.be; Veerle.Cnudde@UGent.be]

Keywords: limestone, salt crystals, salt solutions, segmentation, simultaneous phase-and-amplitude retrieval, synchrotron X-ray micro-computed tomography

ABSTRACT

This paper presents how simultaneous phase-and-amplitude retrieval during X-ray tomographic reconstruction allows a clear segmentation of sodium sulfate solution and hydrated sodium sulfate crystals in Savonnières limestone without the need for a dopant. This technique could be very useful to study salt crystallization processes at the pore scale, in order to improve the understanding and remediation of salt damage in porous media.

1. INTRODUCTION

The crystallization of salts in porous building materials is one of the main causes of deterioration of civil constructions and cultural heritage. One of the key issues is to understand the processes occurring at the pore scale when salt crystals form. The use of synchrotron X-ray micro-computed tomography to study the cooling-induced crystallization of hydrated sodium sulfate crystals in the pore space of a natural stone was investigated (Derluyn 2012). As the attenuation of X-rays by solutions or hydrated phases is low, other researchers used specific salt solutions (*e.g.,* Shokri and Sahimi 2012) or specific particles (*e.g.*, Gaillard *et al.* 2007) to enhance the contrast. We specifically intended to study one of the most damaging salts, sodium sulfate, without altering its nucleation or growth kinetics by adding a dopant. This paper describes the experiment, the image processing needed to distinguish between the different components, *i.e.,* salt solution, hydrated crystals, air and stone, and the resulting visualizations.

2. EXPERIMENTAL WORK

Two cylindrical Savonnières limestone samples, named W and C, of 3.3 mm diameter and ± 5 mm height were investigated by synchrotron radiation X-ray micro-tomographic microscopy. Savonnières is a layered oolitic limestone with a monomineralic calcite composition. The pore system consists of connected micro- (0.1 - 1 µm), meso- (10 µm) and macropores (100 µm range). The samples had a porosity of ± 27 %.

Both samples were taped circumferentially with Kapton (polyimide) tape and glued on the sample holder. Kapton tape is water and vapor tight and transmits X-rays well. The samples were capillary saturated with a 2.8 molal sodium sulfate solution, by bringing the upper side in contact with the

solution for 5 minutes. The solution was put on a hot plate at 40 °C, ensuring undersaturation of the solution with respect to the different crystal phases. This is indicated on the solubility diagram, given in Figure 1a. Sodium sulfate has two stable crystal phases - mirabilite ($Na_2SO_4.10H_20$) and thenardite V ($Na_2SO_4(V)$) - and two metastable crystal phases - heptahydrate ($Na_2SO_4.7H_20$) and thenardite III ($Na_2SO_4(III)$).

After wetting the samples, the top side was closed with a vapor tight mastic paste in order to acquire tomographic datasets without loss of moisture. The first sample, sample W, was scanned in its wet state, in order to study the salt solution distribution in the limestone's pore system. The second sample, sample C, was scanned after being cooled down to – 6 °C. The sample was therefore placed in a closed test chamber that was connected to a cryojet. The cooling process is graphically represented in Figure 1a. It has been often observed in the literature that by cooling, the metastable heptahydrate precipitates first (*e.g.*, Derluyn *et al.* 2011). Heptahydrate typically shows a pyramidal shape, as depicted in Figure 1b.

The datasets were acquired at the TOMCAT beamline of the synchrotron radiation facility Swiss Light Source of the Paul Scherrer Institute, Villigen, Switzerland, using an X-ray photon energy of 32 keV. They consist of 1441 radiographic projection images of 1024 x 664 pixels, with a voxel size of 3.7 µm. The scanning time was around 10 minutes.

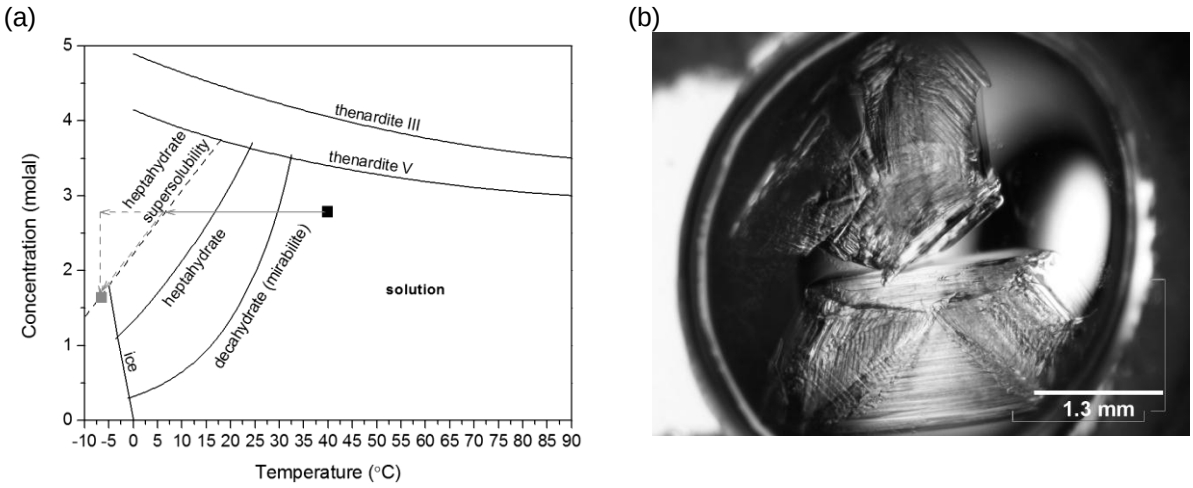

Figure 1: *(a) Sodium sulfate solubility diagram: thenardite, Na_2SO_4(V or III); mirabilite, $Na_2SO_4.10H_2O$; and heptahydrate, $Na_2SO_4.7H_2O$, solubility lines are presented. The cooling of sample C is indicated in gray. (b) Sodium sulfate heptahydrate crystals precipitated in a 2.8 molal sodium sulfate solution at 5 °C.*

3. IMAGE PROCESSING

The tomographic datasets were first reconstructed based on the X-ray absorption of the sample (normal reconstruction, NR), thus based on mixed phase-and-amplitude projection images. Due to the resulting phase artifacts, segmentation between the air and the salt solution and/or hydrated crystal phases could not be obtained from the image histograms. This is illustrated for the sample W in Figure 2a, where the air and the salt solution are lumped together in one peak using the normal reconstruction. To solve this problem, a second reconstruction was done, using simultaneous phase-and-amplitude retrieval (SPAR) (Paganin *et al.* 2002). This algorithm retrieves the sample thickness from the mixed phase-and-amplitude images, thus reducing the phase artifacts. Additionally, the signal-to-noise ratio is improved by using this method (Boone *et al.* 2012). This results in image histograms showing a clear distinction between the different components, as shown in Figure 2a for sample W. All tomographic reconstructions were done using the software Octopus (Vlassenbroeck *et al.* 2007).

The pore space was further analyzed with the software Morpho+ (Brabant *et al.* 2011). This software includes the determination of open and closed pores. Closed pores represent here the pores that are connected via pores with a diameter below the spatial resolution, as these pores cannot be resolved. The obtained spatial resolution resolves fully the macroporosity and partly the mesoporosity of the limestone.

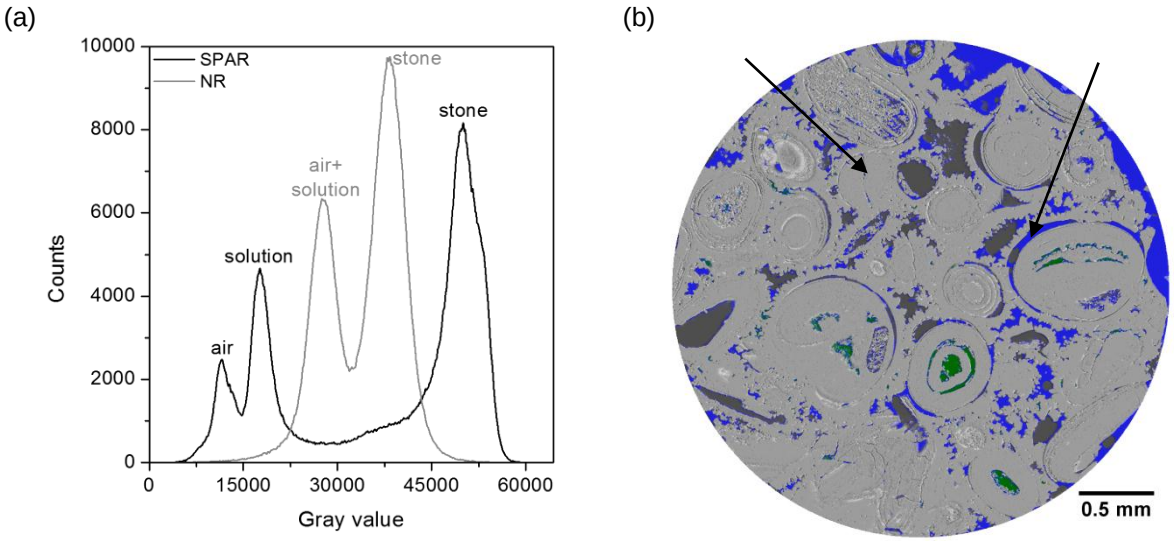

Figure 2: *(a) Histogram of sample W after a normal reconstruction, NR, based on mixed projection images; and after a reconstruction based on simultaneous phase-and-amplitude retrieval, SPAR. (b) Horizontal cross section of sample W, with the solution in blue and the open and closed porosity (with respect to the voxel size of 3.7 µm) in dark gray and green, respectively.*

4. RESULTS AND DISCUSSION

A horizontal cross section of the sample W is shown in Figure 2b. The open porosity is colored in dark gray, the closed porosity in green and the sodium sulfate solution in blue. The solution is present in the open and in the closed pores. Thus, transport into the closed pores occurs, via pores that cannot be resolved, and thus some salt solution is also present in what is seen as the calcite matrix. Figure 2b shows that the oolites are not always well connected with the surrounding calcite matrix, creating pore space, and that microcracks can be present in oolites, into which the salt solution can penetrate (indicated by the left arrow). The macropores inside the oolites and in between the calcite cement are not completely filled by the solution, but a liquid film is formed on the surface. The meniscus can be observed, *e.g.*, as indicated by the arrow on the right.

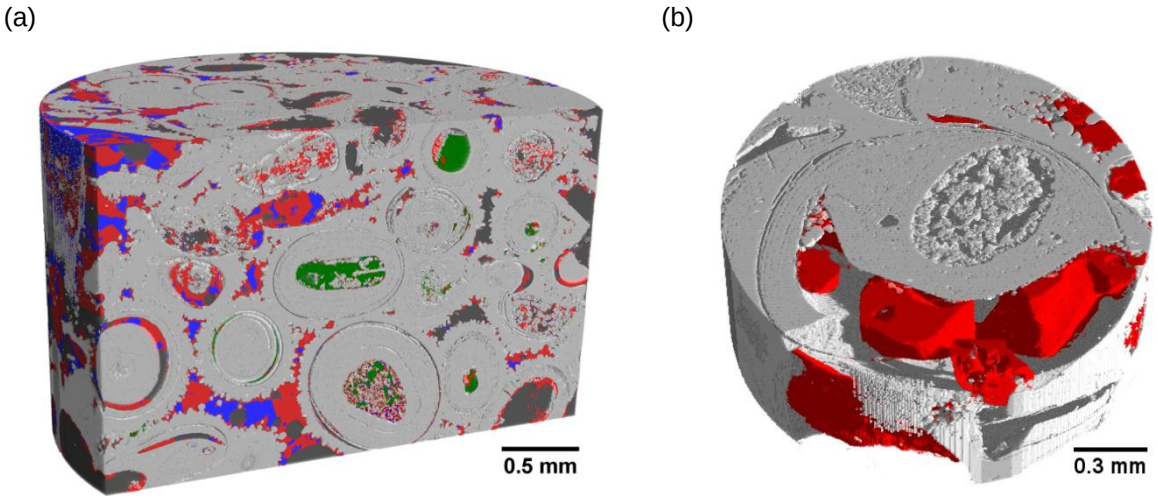

Figure 3: *(a) Distribution of hydrated sodium sulfate crystals, in red, and salt solution, in blue, after cooling sample C. The open and closed porosity (with respect to the voxel size of 3.7 µm) are represented in dark gray and green, respectively. (b) Close-up of a macropore in sample C. The crystal shape suggests that the hydrated crystal is sodium sulfate heptahydrate.*

A vertical cross section of the sample C is given in Figure 3a. The image shows the state of the sample after 30 minutes of cooling. The hydrated crystal phase is colored in red and the surrounding salt solution in blue. We observe that large hydrated crystals can form in the macropores; a close-up

of one macropore is given in Figure 3b. The crystal shape has a (bi)pyramidal structure, which is the shape reported for heptahydrate crystals. We also observe smaller crystals inside oolites that still have a porous structure in their center; some of these pores are characterized as closed porosity, given the resolution of the dataset.

The results suggest that salt crystals precipitate in all pore systems of Savonnières limestone. Crystals can partly fill the macropores as they can grow from the liquid film present on the pore wall. Crystals can grow in mechanically weak zones of the stone, where there is less cohesion between the oolites and the calcite cement or where there is less cohesion between the calcite grains. Consequently, it is not remarkable that, under such a distributed occurrence of salt growth, damage can occur (Derluyn 2012).

5. CONCLUSIONS

We have shown that using simultaneous phase-and-amplitude-retrieval during reconstruction of a monomineralic limestone allows a clear segmentation of salt solution, hydrated salt crystals and air in its pore space. No contrast enhancement by the use of a specific salt or a dopant is needed, by which the crystallization kinetics remain unaltered. This technique could be useful to study crystallization or freezing processes in the future within pore systems of, *e.g.*, building materials.

6. ACKNOWLEDGEMENTS

This work is based on experiments performed at the TOMCAT beamline at the Swiss Light Source, Paul Scherrer Institute, Villigen, Switzerland. The technical help of Gordan Mikuljan and the assistance of Michele Griffa, Tim De Kock, Sevi Modestou and Peter Modregger during the beamtime are greatly appreciated. IWT-Flanders is acknowledged for its grant to Jan Dewanckele.

7. REFERENCES

Boone, M. N., De Witte, Y., Dierick, M., Almeida, A. and Van Hoorebeke, L. (2012). Improved Signal-to-Noise Ratio in Laboratory-Based Phase Contrast Tomography. Microscopy and Microanalysis, 18 (2), 399-405.

Brabant, L., Vlassenbroeck, J., De Witte, Y., Cnudde, V, Boone, M. N., Dewanckele, J. and Van Hoorebeke, L. (2011). Three-dimensional analysis of high-resolution X-ray computed tomography data with Morpho+. Microscopy and Microanalysis, 17 (2), 252–263.

Derluyn, H., Saidov, T. A., Espinosa-Marzal, R. M., Pel, L. and Scherer, G. W. (2011). Sodium sulfate heptahydrate I: The growth of single crystals. Journal of Crystal growth, 329, 44-51.

Derluyn, H. (2012). Salt transport and crystallization in porous limestone: neutron – X-ray imaging and poromechanical modeling. Dissertation ETH No. 20673, ETH Zurich, Switzerland.

Gaillard, J.-F., Chen, C., Stonedahl, S. H., Lau, B. L. T., Keane, D. T. and Packman, A. I. (2007). Imaging of colloidal deposits in granular porous media by X-ray difference micro-tomography. Geophysical Research Letters, 34, L18404.

Paganin, D., Mayo, S. C , Gureyev, T. E., Miller, P. R. and Wilkins, S. W. (2002). Simultaneous phase and amplitude extraction from a single defocused image of a homogeneous object. Journal of Microscopy, 206, 33–40.

Shokri, N and Sahimi, M. (2012). Structure of drying fronts in three-dimensional porous media. Physical Review E, 85, 066312.

Vlassenbroeck, J., Dierick, M., Masschaele, B., Cnudde, V., Van Hoorebeke, L. and Jacobs, P. (2007). Software tools for quantification of x-ray microtomography at the UGCT, Nuclear Instruments and Methods in Physics Research Section A: Accelerators, Spectrometers, Detectors and Associated Equipment, 580, 442–445.